Volume 31 (2012), Number 0 pp. 1–12 COMPUTER GRAPHICS *forum*

Extraction of Dominant Extremal Structures in Volumetric Data using Separatrix Persistence

D. Günther, H.-P. Seidel and T. Weinkauf

Max Planck Institute for Informatics, Saarland University, Saarbrücken, Germany

Abstract

Extremal lines and surfaces are features of a 3D scalar field where the scalar function becomes minimal or maximal with respect to a local neighborhood. These features are important in many applications, e.g., computer tomography, fluid dynamics, cell biology. We present a novel topological method to extract these features using discrete Morse theory. In particular, we extend the notion of Separatrix Persistence *from 2D to 3D, which gives us a robust estimation of the feature strength for extremal lines and surfaces. Not only does it allow us to determine the most important (parts of) extremal lines and surfaces, it also serves as a robust filtering measure of noise-induced structures. Our purely combinatorial method does not require derivatives or any other numerical computations.*

Categories and Subject Descriptors (according to ACM CCS): I.4.7 [Image Processing and Computer Vision]: Feature Measurement—Feature representation

1. Introduction

Scalar fields are the results of measurements and numerical simulations and essential to understanding processes in many domains. Examples are imaging techniques in medicine such as MRI or CT scans, electron tomography in cell biology, or derived scalar quantities in fluid dynamics. Scalar fields are visualized and analyzed using a large number of tools. Established visualization choices include volume rendering or isosurfaces.

Among the features of interest in a 3D scalar field are extremal lines and surfaces at which the scalar function becomes minimal or maximal with respect to a local neighborhood. For example, vortex core lines can be found in a flow data set as lines where the Q-criterion becomes maximal [SWTH07]. Blood vessels appear as lines of maximal intensity in computer tomography data. In cell biology, the membrane of a cell can be found as a surface of minimal density [RGH*12] in an electron tomography volume. Note that the scalar value varies along these lines and surfaces.

Two different concepts are commonly used for extracting extremal structures: the local analysis due to ridges/valleys and the global point of view by means of topology. In this paper, we concentrate on the topological view, but will also provide a brief discussion of the similarities and differences to ridges/valleys (Section 2).

The topologically motivated extremal structures of a regular 3D scalar field f are given by the Morse-Smale (MS) complex: it is comprised of points, lines, and surfaces. They provide a segmentation of the domain into monotone cells [Mil63] (Section 3). Each cell is cornered by non-degenerated critical points (a minimum, a maximum, and saddle points). The boundaries between cells are provided by separation lines and surfaces – so-called *separatrices*.

Two types of approaches exist to extract the MS complex. The continuous approach [NS94, Wei08] builds on the gradient $\mathbf{g}$ and Hessian $\mathbf{H}$ of f. Noise in f and its amplification in $\mathbf{g}$ and $\mathbf{H}$ pose a numerical challenge. The discrete approach due to Forman's *discrete Morse theory* [For98] works on sampled data only, but does not require any derivatives or other numerical computations, since it describes the MS-complex in a purely combinatorial fashion. So while noise is less of a problem due to the exclusion of derivatives, spurious extraction results still show up because of the noise level in the original data f. Hence, filtering is necessary.

A well-accepted filtering criterion for critical points is *persistence* due to Edelsbrunner et al. [ELZ02] (Section 3). The separation lines of a 2D scalar field can be filtered using a closely related measure called *separatrix persistence* [WG09], which determines the feature strength of a separatrix or parts thereof. However, such a measure does not yet exist for the separation lines and surfaces of a 3D scalar field.

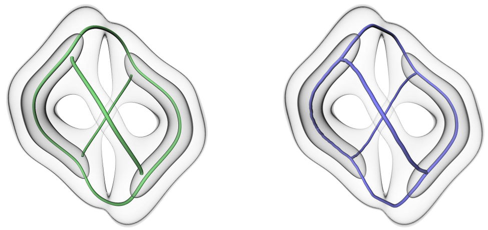

Figure 1: Extremal lines of a 3D scalar field following two different definitions: ridges (left) and separatrices (right).

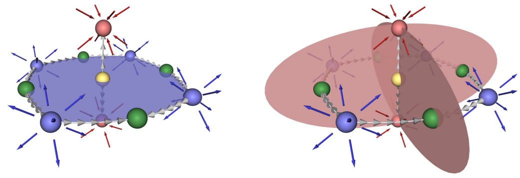

Figure 2: An illustration of topological features. Minima, repelling and attracting saddles, and maxima are depicted as blue, green and yellow, and red spheres. Attracting and repelling surfaces are shown in blue and red, respectively.

In this paper, we extend the approach of [WG09] and introduce separatrix persistence for the separation lines and surfaces of 3D scalar fields (Section 4). To the best of our knowledge, it is the first topologically motivated measure of feature strength for separatrices of a 3D scalar field. It is a non-trivial extension of [WG09], since it requires a consistent definition for both lines and surfaces in 3D, whereas for 2D scalar fields it is only defined for lines. We comment on implementational issues (Section 5), and apply our method to data sets from different domains (Section 6).

2. Separatrices vs. Height Ridges

A minimal/maximal *point* is canonically defined in arbitrary dimensions. However, its higher-dimensional generalizations cannot be defined in a canonical way, i.e., several equated definitions exist for extremal *lines* or *surfaces*. This is documented throughout the literature [Kv93, Dam99, LLSV99, SWTH07, PS08, SPFT12]. Besides their global definition as topological separatrices [Max70], another frequently used concept are *Height Ridges*, which goes back to De Saint-Venant [dSV52]. We will briefly recapitulate their definition and discuss similarities and differences to topological separatrices.

The Height Ridge definition [Ebe96] is a local definition and builds on the first and second derivatives of f, i.e., the gradient $\mathbf{g}$ and the Hessian $\mathbf{H}$. As elegantly formulated by Peikert and Sadlo [PS08], ridge lines in a 3D scalar field are found at locations where the vectors $\mathbf{g}$ and $\mathbf{H}\cdot\mathbf{g}$ are parallel. They can be extracted using the Parallel Vectors operator [PR99, POS*11]. Ridge surfaces can be found as parts of the zero level set $\mathbf{g}\cdot\mathbf{e}_1$ with $\lambda_1 < 0$, where $\mathbf{e}_1$ is the eigenvector to the smallest eigenvalue λ_1 of $\mathbf{H}$. A consistent orientation of the eigenvectors at the vertices of each cell is necessary to extract this level set. This can be achieved using a principal component analysis [FP01].

Figure 1 shows the ridge lines (left) and separation lines (right) of a 3D scalar field. It can be seen that they largely coincide and that both are in the center of the shown isosurfaces. which confirms their extremal characteristic.

It has been pointed out by Sahner et al. [SWTH07] that every separatrix can be assigned a ridge counterpart: each saddle point of f gives rise to ridges as well as separatrices (they do not need to coincide at any other places). However, not every ridge can be assigned a separatrix counterpart [SWTH07]. Intuitively, this happens when a ridge-creating fluctuation of f does not break its monotony. This is nicely shown by the "Ridges without Critical Points" example of Peikert and Sadlo [PS08].

By definition, separation lines are tangential to the gradient $\mathbf{g}$. Ridges lines, on the other hand, are defined as features where $\mathbf{g}$ is parallel to $\mathbf{H}\cdot\mathbf{g}$. In fact, additionally requiring that they are also tangential to $\mathbf{g}$ yields an overdetermined system as discussed by Schindler et al. [SPFT12]. However, in some applications, ridge lines should roughly point into the direction of $\mathbf{g}$. Peikert and Sadlo [PS08] proposed a filter criterion F_α based on the angle α between the ridge line and the gradient. Typically, α varies between 5° and 60°.

There are several differences between ridges and separatrices from an algorithmic point of view: ridges are local features, which eases their extraction using parallel algorithms. This might be difficult for separatrices due to their global nature. On the other hand, separatrices can be extracted combinatorially without any derivatives as it is shown in this paper. Ridge lines depend on the computation of first and second derivatives, which usually causes a wealth of spurious extraction results. In Section 6, we compare our topological extraction results against ridge lines/surfaces.

3. Theoretical Background

In this section, we discuss the for our purposes most important terms of topology, discrete Morse theory, and persistence. We assume that a Morse-Smale function $f : \Omega \to \mathbb{R}$ with $\Omega \subset \mathbb{R}^3$ is given [Sma60]. To ease notation in the following, we define the *height difference* h of two points $\mathbf{x} \in \mathbb{R}^3$ and $\mathbf{y} \in \mathbb{R}^3$ as

$$h(\mathbf{x},\mathbf{y}) = |f(\mathbf{x}) - f(\mathbf{y})|. \quad (1)$$

3.1. Topological Features

The topological features of a 3D Morse-Smale function f consist of non-degenerated critical points, separation lines

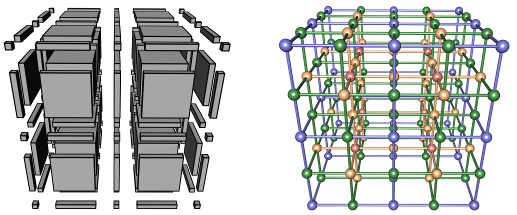

Figure 3: Illustration of a cubical cell complex C and its derived cell graph G. The nodes of G represent the 0-, 1-, 2-, and 3-cells of C and are shown as blue, green, yellow, and red spheres, respectively.

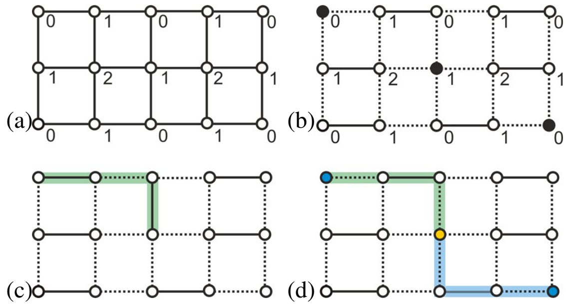

Figure 4: Basic definitions of discrete Morse theory: (a) the cell graph G, each node is labeled by its dimension; (b) a combinatorial gradient field V defined on G, the edges contained in V are depicted by solid lines, the critical nodes – are shown as black spheres; (c) a combinatorial streamline; (d) two separatrices of V (blue and green) emanating at a saddle (yellow) and ending in two different minima (blue).

and separation surfaces. For their numerical treatment, we refer to [Wei08].

There are four types of critical points: *minima*, *repelling saddles*, *attracting saddles*, and *maxima*. Considering an increasing isovalue, the critical points are closely related to the evolution of connected components, tunnels, and voids of isocontours. The births and deaths of these elements are described by the critical points [Mil65]. For example, a connected component is born at a minimum. A tunnel, on the other hand, is born at a repelling saddle when a component forms a closed loop with itself.

Two *separation lines* emerge from each saddle point, which are streamlines in the underlying gradient field. They connect a repelling saddle to at most two minima, while an attracting saddle is connected to at most two maxima. We call these lines *minimal lines* and *maximal lines*, resp..

In addition to separation lines, a *separation surface* emanates from each saddle point, which is a set of streamlines in the underlying gradient field. We call it a *repelling surface* if it emanates from a repelling saddle, and *attracting surface* otherwise. The boundary of a separation surface consists of separation lines and critical points. An attracting surface is bounded by repelling saddles and their minimal lines (Figure 2 left). A repelling surface, on the other hand, is bounded by attracting saddles and their maximal lines (Figure 2 right).

The non-degenerated critical points, separation lines and surfaces give rise to the Morse-Smale (MS) complex that decomposes the domain Ω into compartments where f behaves monotonically [Mil63]. The border between two adjacent compartments constitutes a change of that monotony, and is given by a separatrix. In this sense, separatrices have an extremal characteristic.

3.2. Discrete Morse Theory

We now give a brief introduction to discrete Morse theory. The interested reader is referred to the seminal work of Forman [For98, For02] for a more thorough description of this theory. For computational aspects we refer to [LLT03, Lew12, GNP*05, GRWH11, GRP*12].

The input domain Ω is given in a discretized manner. Common discretizations are lattices or tetrahedrizations. The discretization gives rise to a finite regular *cell complex* C [Hat02]. This complex consists of cells with different dimensions (e.g., vertices, edges, faces, volumina) and of boundary maps describing their neighborhood relation. For example, an edge is bounded by its two incident vertices, whereas a face is bounded by its incident edges. An illustration of a cell complex is given in Figure 3 left.

We consider the cell complex C in a graph theoretical setting: the *cell graph* $G = (N,E)$ encodes the essential combinatorial information of C. The nodes N represent the cells of C and each node $\mathbf{u}^p$ is labeled by the dimension p of the cell it represents. The edges E encode the neighborhood relation of the cells. If a cell $\mathbf{u}^p$ is in the boundary of a cell $\mathbf{w}^{p+1}$, then $e^p = \{\mathbf{u}^p, \mathbf{w}^{p+1}\} \in E$. The edge e^p is said to be of index p. A depiction of a cell graph is shown in Figure 3 right.

A subset of pairwise non-adjacent edges is called a matching. A *combinatorial gradient field* $V \subset E$ on a regular cell complex C can now be defined as a matching of the cell graph G with a certain acyclic constraint [Cha00]. We will define this constraint later in this section.

In this combinatorial setting, the critical points are the unmatched nodes of V. A critical point $\mathbf{u}^p$ of index p is a minimum $(p=0)$, repelling saddle $(p=1)$, attracting saddle $(p=2)$, or maximum $(p=3)$.

A *combinatorial p-streamline* is a path in the cell graph G whose edges are of index p and alternate between V and its complement $E \setminus V$. The above mentioned acyclic constraint is now specified as the non-existence of any closed p-streamline. A p-streamline connecting two critical points

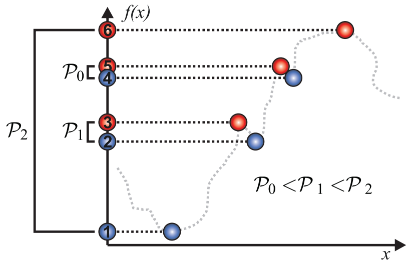

Figure 5: Persistence $\mathcal{P}$ of a 1D function $f(x)$. Sweeping through the data in an ascending manner collects the minima (blue) and maxima (red) in the shown order. Every maximum is paired with a preceding minimum and their height difference is their persistence. Note how the global minimum and maximum have been assigned the highest persistence.

$\mathbf{u}^p$ and $\mathbf{w}^{p+1}$ is called a *combinatorial p-separation line*. A 0-separation line is a minimal line, whereas a 2-separation line represents a maximal line. A *combinatorial separation surface* is given by all combinatorial 1-streamlines that emanate from a repelling or attracting saddle. Note that combinatorial extremal lines and surfaces are given as discrete sets of edges in G in contrast to their continuous counterparts.

Figure 4 shows a simple cell graph, a combinatorial gradient field and its combinatorial structures. For the sake of simplicity, this is shown in 2D.

3.3. Persistence

An established importance measure for critical points is persistence $\mathcal{P}$. Considering an increasing isovalue, it measures the "life time" of connected components, tunnels, and voids of the isocontours of f. The birth and death events are described by pairs of critical points. For simplicity, Figure 5 illustrates this for the 1D case. We refer the reader to [ELZ02] for the more general case.

An important property of persistence is given by the stability theorem of Cohen-Steiner et al. [CSEH07]. They proved that persistence behaves stable under small perturbations of the input function. This property allows for the distinction of noise-induced and dominant critical points.

3.4. Topological Simplification

Topologically simplifying a combinatorial gradient field V means to reduce the number of its critical points in order to create different levels of detail of the input function f. All fine-grained topological features are present in the initial gradient field V, while the last level contains only the dominant topological features of the scalar field f.

Such a hierarchy can be achieved by increasing the set of edges in V without introducing any closed p-streamlines as discussed by Forman [For98]. Consider two critical points

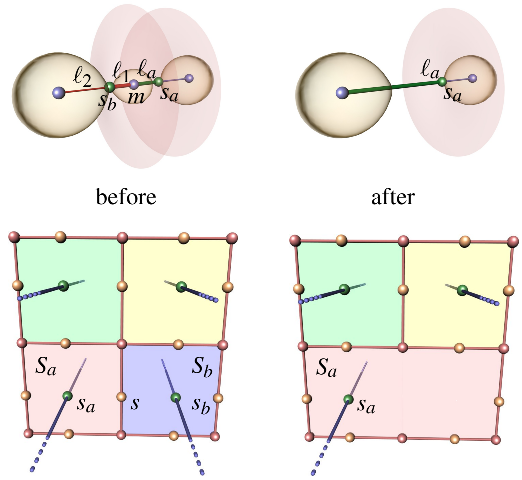

Figure 6: Simplification increases the length (top row) and area (bottom row) of affected extremal lines and surfaces. Shown are the extremal structures before (left) and after (right) a simplification.

$\mathbf{u}^p$ and $\mathbf{w}^{p+1}$ that are connected by a single p-separation line q. This line is given as a sequence of alternating edges that belong either to $E \setminus V$ or V. Taking the symmetric difference $\tilde{V} = V \triangle q$ yields a new combinatorial gradient field $\tilde{V}$ with an increased set of edges where $\mathbf{u}^p$ and $\mathbf{w}^{p+1}$ are not critical anymore, i.e., the edges incident to these points are now matched. Note that this operation does not create any cycles as long as there is a unique path connecting the two critical points [For98].

The symmetric difference not only removes two critical points from a combinatorial gradient field, it also increases the length/area of the affected p-separatrices. The extremum-saddle simplification (s_b, m) in the top row of Figure 6 yields a merge of the separation lines ℓ_1, ℓ_2 with ℓ_a: the length of ℓ_a is increased while ℓ_1 and ℓ_2 are removed. The saddle-saddle simplification (s, s_b) in the lower row of Figure 6, on the other hand, increases the area of the separation surface S_a: the surface S_b merges into S_a.

A hierarchy of combinatorial gradient fields $(V_i)_{i=0...m}$ could be obtained by iteratively taking the symmetric difference with respect to the persistence pairs (Section 3.3). However, this symmetric difference does not necessarily yield a combinatorial gradient field where upcoming persistence pairs can be canceled in the sense of Forman, as extensively discussed by Bauer et al. [BLW11]: a necessary property to reduce the number of critical points in the sense of Forman is collapsibility of a discrete Morse function, but this is not always given for a generic 3D Morse function.

The above theoretical argument results, in practice, in the following situation: when creating a hierarchy in the order of the persistence pairs, one arrives rather early in a deadlock

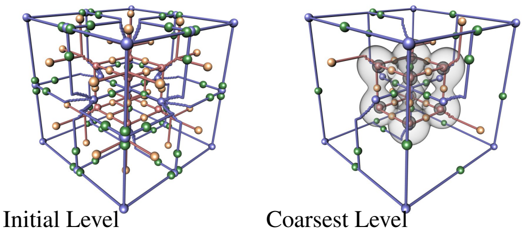

Figure 7: Persistence-based simplification. Shown are the extremal structures of the initial field V_0 (left) and the final field V_m (right), which still contains critical points. Gray isosurfaces illustrate the underlying synthetic function.

where a unique p-separation line between two paired critical points does not exist. An artificial example is shown in Figure 7. The input function consists of 129 critical points. However, only the first 32 persistence pairs could be removed using the symmetric difference. The coarsest representation of the input function still contains 65 critical points. In fact, it follows from Joswig et al. [JP06] that it is an NP-hard problem to pair critical points such that V_m contains the minimal number of critical points, which itself is given by the topology of the domain (for a uniform lattice this is a sole minimum).

In this paper, we use the greedy strategy proposed by Günther et al. [GRP*12] for pairing critical points. The main idea is to apply the symmetric difference to a pair representing the current smallest fluctuation in the data. This greedy approach is motivated by the fact that persistence pairs coincide with *smallest fluctuation pairs* for 2D Morse functions [DLL*10].

Given a certain level of the hierarchy V_i, we are looking for the pair of critical points $\{\mathbf{u}^p, \mathbf{w}^{p+1}\}$ that is connected by a unique p-separation line q and represents the smallest height difference $h(\mathbf{w}^{p+1}, \mathbf{u}^p)$ of all possible pairs. The symmetric difference

$$V_{i+1} = V_i \triangle q \tag{2}$$

yields the simplified field V_{i+1}. Applying (2) iteratively gives the hierarchy $(V_i)_{i=0...m}$.

In practice, we found that this greedy approach is able to pair more critical points than a persistence-based simplification. In the above example (cf. Figure 7) all critical points are paired with this approach and a sole minimum remains in V_m. The greedy approach leads to longer separation lines and larger separation surfaces in the coarsest level of the hierarchy. The coarsest level using the persistence pairing, on the other hand, may contain a large number of unimportant critical points. This influences the computation of separatrix persistence and may lead to an underestimation of the importance as discussed in Section 4.

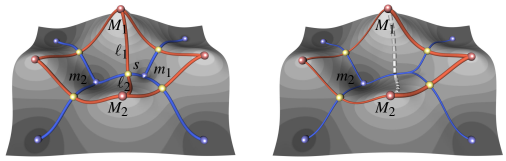

Figure 8: Illustration of the 2D simplification process. Shown is the 2D Morse-Smale complex before the simplification (left), and after the simplification (right). Images taken from [WG09] with permission of the authors.

3.5. Separatrix Persistence in 2D

Separatrix persistence was originally introduced for scalar functions defined on a 2D manifold and has been used to extract salient edges on surfaces meshes [WG09]. It quantifies the feature strength for each point on a 2D separation line individually. This enables the distinction of spurious and dominant *parts* of a separation line. In contrast, topological simplification removes only *whole* separatrices.

Let $\mathbf{s}$ denote a saddle. Four separatrices emanate from $\mathbf{s}$: two minimal lines connecting $\mathbf{s}$ to at most two minima $\mathbf{m}_i$, and two maximal lines connecting $\mathbf{s}$ to at most two maxima $\mathbf{M}_i$. We assume that $(\mathbf{s}, \mathbf{m}_1)$ is a persistence pair that causes a simplification of the underlying gradient field. The simplification removes the critical points $\mathbf{s}$ and $\mathbf{m}_1$ as well as the maximal lines. Figure 8 shows this. Let ℓ_1 and ℓ_2 denote the two removed maximal lines. For each point $\mathbf{x} \in \ell_1 \cup \ell_2$, the 2D separatrix persistence $\mathcal{S}_{2D}$ has originally been defined in [WG09] as follows

$$\mathcal{S}_{2D}(\mathbf{x}) = f(\mathbf{x}) - f(\mathbf{m}_1), \tag{3}$$

with a similar statement holding for minimal lines. The feature strength of all points of all separation lines is computed during a continued simplification process until no further simplification is possible.

To ease the extension to 3D, we stress that $h(\mathbf{x}, \mathbf{m}_1) = h(\mathbf{x}, \mathbf{s}) + h(\mathbf{s}, \mathbf{m}_1)$. Note that the same statement holds for minimal lines by considering $h(\mathbf{M}_1, \mathbf{x})$. Additionally, the identity $h(\mathbf{s}, \mathbf{m}_1) = \mathcal{P}(\mathbf{s}) = \mathcal{P}(\mathbf{m}_1)$ is given for each persistence pair $(\mathbf{s}, \mathbf{m}_1)$. We rewrite (3) in an equivalent form, which now applies to both minimal and maximal lines using the same notation:

$$\mathcal{S}_{2D}(\mathbf{x}) = \mathcal{P}(\mathbf{s}) + h(\mathbf{x}, \mathbf{s}). \tag{4}$$

4. Separatrix Persistence in 3D Scalar Fields

In the following, we extend the notion of *separatrix persistence* from 2D to 3D. It will allow us to measure the feature strength of the separatrices in the 3D MS-complex, i.e., the extremal lines and surfaces of a 3D scalar field. Separatrix persistence will be used to filter less significant or noise-induced (parts of) extremal lines and surfaces. This is es-

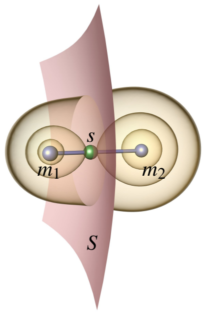

Figure 9: Illustration of the local feature strength of separation surfaces. The evolution of isocontours is depicted as yellow surfaces.

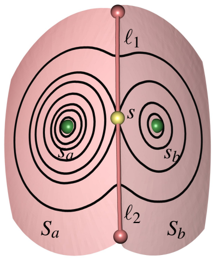

Figure 10: Illustration of the local feature strength of separation lines. The evolution of isolines is depicted as black lines.

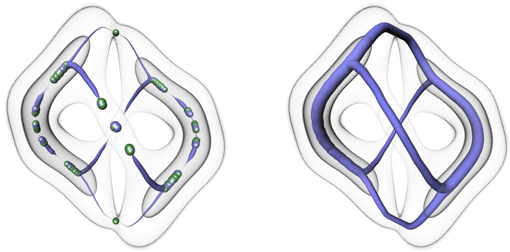

Figure 11: Extremal lines scaled by local feature strength (left) and separatrix persistence (right). Small fluctuations in the data cause an improper representation of the dominant extremal structures using the local feature strength. Separatrix persistence, in contrast, reveals the global structure.

pecially important when the coarsest level of (V_i) still contains topological information (Section 3.4). Separatrices that mainly describe artificial features may be present. Our measure will enable us to keep only the relevant parts of them. Separatrix persistence is derived from the persistence of critical points and inherits its stability under small perturbations of the input function.

Similar to the persistence of critical points, separatrix persistence builds on the behavior of isocontours when considering an increasing isovalue. Based on this behavior, we will define the *local strength of separation* for the separatrices of a *single* saddle, i.e., for its separation surface and its two separation lines (Section 4.1). This local measure will be the foundation for the definition of *separatrix persistence* in a 3D scalar field (Section 4.2).

4.1. Local Strength of Separation

Consider a single repelling saddle $\mathbf{s}$ and its repelling separation surface S as shown in Figure 9. The separation surface is the boundary between the two volumes governed by the minima $\mathbf{m}_1$ and $\mathbf{m}_2$. Our goal is to define the strength of this separation for each point on S. To do so, we observe how the evolution of an isocontour affects the separation between the volumes. Let $f(\mathbf{m}_1) > f(\mathbf{m}_2)$. Also note that $f(\mathbf{s}) > f(\mathbf{m}_1)$ by construction. For an increasing isovalue r, we have the following behavior for the isocontour:

zero components	$r < f(\mathbf{m}_2) < f(\mathbf{m}_1) < f(\mathbf{s})$
one component around $\mathbf{m}_2$	$f(\mathbf{m}_2) \leq r < f(\mathbf{m}_1) < f(\mathbf{s})$
two components around $\mathbf{m}_1$ and $\mathbf{m}_2$	$f(\mathbf{m}_2) < f(\mathbf{m}_1) \leq r < f(\mathbf{s})$
the two components merge at the saddle $\mathbf{s}$	$f(\mathbf{m}_2) < f(\mathbf{m}_1) < r = f(\mathbf{s})$
one component intersecting the separation surface	$f(\mathbf{m}_2) < f(\mathbf{m}_1) < f(\mathbf{s}) < r$

The separation surface is pierced by the isocontour for the first time when the two components merge at the saddle. This infinitesimal small hole constitutes a breach of the separation between the two volumes. In other words, the saddle is the weakest point of separation between the two volumes. With further increasing r, the hole becomes larger, and we find that the outer parts of S provide the strongest separation between the volumes. Mathematically speaking, we define the local strength of separation $\mathcal{I}_S$ for all points $\mathbf{x} \in S$ as

$$\mathcal{I}_S(\mathbf{x}) = \mathcal{P}(\mathbf{s}) + h(\mathbf{x}, \mathbf{s}), \tag{5}$$

which has its smallest value at the saddle: $\mathcal{I}_S(\mathbf{s}) = \mathcal{P}(\mathbf{s})$ denotes the persistence of $\mathbf{s}$ and thereby the "life time" of the weakest point on the separation surface. Note that $\mathcal{P}(\mathbf{s}) = \mathcal{P}(\mathbf{m}_1) = h(\mathbf{s}, \mathbf{m}_1)$, if $(\mathbf{s}, \mathbf{m}_1)$ is a persistence pair, which is the case in a simple scalar field as described above. In the next section, we will consider scalar fields with more topological structures, where $(\mathbf{s}, \mathbf{m}_1)$ may not be a persistence pair. A statement similar to (5) holds for attracting surfaces.

The definition for the two separation lines ℓ_1, ℓ_2 of a saddle $\mathbf{s}$ follows the same ideas, except that these lines do not separate volumes, but areas on two neighboring separation surfaces S_a, S_b coming from two saddles $\mathbf{s}_a, \mathbf{s}_b$ with $f(\mathbf{s}_a) > f(\mathbf{s}_b)$ (Figure 10). Therefore, we observe the evolution of isocontours of f restricted to these surfaces, i.e., we consider isolines. They emanate at $\mathbf{s}_a$ and $\mathbf{s}_b$, merge at $\mathbf{s}$, and create an increasingly larger hole in ℓ_1 and ℓ_2. It turns out, we can define the local strength of separation $\mathcal{I}_\ell$ for all points $\mathbf{x} \in \ell_1 \cup \ell_2$ very similarly to (5):

$$\mathcal{I}_\ell(\mathbf{x}) = \mathcal{P}(\mathbf{s}) + h(\mathbf{x}, \mathbf{s}). \tag{6}$$

Note that $\mathcal{P}(\mathbf{s}) = \mathcal{P}(\mathbf{s}_a) = h(\mathbf{s}, \mathbf{s}_a)$, if $(\mathbf{s}, \mathbf{s}_a)$ is a persistence pair.

4.2. Definition of Separatrix Persistence

The objective of this paper is to define a measure that allows to filter the separation lines and surfaces of the MS complex such that only the ones with the strongest separating behavior remain. A naïve approach would be to use the local strengths of separation $\mathcal{I}_\ell$ and $\mathcal{I}_S$ directly on the unsimplified

MS complex. However, taking only the locally connected critical points into consideration does not accommodate the global gestalt of the function; as shown in Figure 11 left for a synthetic data set. Local perturbations cause an erratic and unintuitive behavior of $\mathcal{I}_\ell$ and $\mathcal{I}_S$ – if applied directly to the unsimplified MS complex.

We use the hierarchy of combinatorial gradient fields $(V_i)_{i=0\ldots m}$ from Section 3.4 to successively remove small perturbations and gain an increasingly global view of the topological features. Note that the connectivity of critical points changes within (V_i). Additionally, combinatorial separation lines and surfaces may merge during the simplification process. A point $\mathbf{x}$ on a separatrix can therefore separate multiple critical points. Hence, we need to determine the *maximal* strength of separation for $\mathbf{x}$ by considering (5) and (6) over all elements of (V_i). We define for separation surfaces:

Definition 1 (Separatrix Persistence for Surfaces) Let S_i be the separation surface of a saddle $\mathbf{s}_i$ at a hierarchy level i. At most two extrema are connected to $\mathbf{s}_i$: let $\mathbf{e}_i$ denote the extremum with the smallest persistence. The *Separatrix Persistence* $\mathcal{S}$ is defined for each point $\mathbf{x} \in S_i$ as

$$\mathcal{S}(\mathbf{x}) = \max_{i=0,\ldots,m} \left(\mathcal{P}_{\max}(\mathbf{s}_i, \mathbf{e}_i) + h(\mathbf{x}, \mathbf{s}_i)\right), \tag{7}$$

where $\mathcal{P}_{\max}(.,.)$ denotes the maximal persistence of two critical points.

In other words, $\mathcal{S}(\mathbf{x})$ is the *largest* strength of separation that could be found over *all* hierarchy levels at the point $\mathbf{x}$. This corresponds to (cf. Equation (5))

$$\begin{aligned} \mathcal{S}(\mathbf{x}) &= \max_i \left(\mathcal{I}_{S_i}(\mathbf{x})\right) && (8)\\ &= \max_i \left(\mathcal{P}(\mathbf{s}_i) + h(\mathbf{x}, \mathbf{s}_i)\right) && (9)\\ &= \max_i \left(\mathcal{P}(\mathbf{e}_i) + h(\mathbf{x}, \mathbf{s}_i)\right) && (10) \end{aligned}$$

but only if the saddle-extremum pairs $(\mathbf{s}_i, \mathbf{e}_i)$ obtained through the hierarchy are actually persistence pairs. As discussed in Section 3.3 as well as in [BLW11], this is not necessarily the case in 3D scalar fields. This may yield the situation that a saddle point with a low persistence is connected to an extremum with a high persistence. Taking only the persistence of the saddle into account would result in an underestimation of the emerging separatrices. We therefore use the maximum of persistence $\mathcal{P}_{\max}(\mathbf{s}_i, \mathbf{e}_i)$ in (7) of two neighboring critical points $(\mathbf{s}_i, \mathbf{e}_i)$, since it estimates the largest strength of separation.

Note that a separatrix exists only up to a level V_j in the hierarchy (V_i). Hence, (7) is effectively computed for the levels $V_0, \ldots, V_j$, and not further examined for levels $k > j$.

Separatrix persistence for separation lines follows a similar scheme:

Definition 2 (Separatrix Persistence for Lines) Let ℓ_i be a separation line of a saddle $\mathbf{s}_i$ at a hierarchy level i. The separation surface of $\mathbf{s}_i$ has several other saddles in its boundary: let $\mathbf{t}_i$ denote the one with the smallest persistence. The *Separatrix Persistence* $\mathcal{S}$ is defined for each point $\mathbf{x} \in \ell_i$ as

$$\mathcal{S}(\mathbf{x}) = \max_{i=0,\ldots,m} \left(\mathcal{P}_{\max}(\mathbf{s}_i, \mathbf{t}_i) + h(\mathbf{x}, \mathbf{s}_i)\right). \tag{11}$$

Figure 11 right shows the minimal lines of a synthetic data set that have been scaled by separatrix persistence.

Table 1: Time needed to compute the initial MS-complex (1), persistence of critical points (2), and the hierarchy (V_i) including separatrix persistence (3). The number of critical points after $\varepsilon = 10\%$ simplification is given in the second column.

Data set (Resolution)	# Crits $\varepsilon = 10\%$	(1) (min)	(2) (min)	(3) (min)
Bonsai (256^3)	3905	1	5	9
Aneurism (256^3)	8549	1	< 1	2
Cylinder Flow ($265 \times 337 \times 65$)	43	< 1	< 1	< 1
Filopodium ($124 \times 154 \times 47$)	8521	< 1	< 1	5

4.3. Computing Separatrix Persistence

A straightforward approach in computing $\mathcal{S}(\mathbf{x})$ is to iterate over each saddle $\mathbf{s}_i$ in each level of the hierarchy $(V_i)_{i=0\ldots m}$ and compute (7) and (11) for each point $\mathbf{x}$ on the separatrices of $\mathbf{s}_i$. However, a more efficient approach is possible by exploiting that a simplification step $V_i \to V_{i+1}$ creates only local changes in the MS-complex (Section 3.4): only one pair of critical points gets removed with every simplification step. Hence, we compute (7) and (11) only for the separatrices that are affected in this step; and continue to the next level in the hierarchy. At V_m, we evaluate (7) and (11) for the separatrices of the (few) remaining saddles. Since separatrices are given as discrete set of edges in the cell graph G, we assign the importance values only to the nodes incident to these edges. An explicit sampling of separatrices is not necessary. This makes computing separatrix persistence very efficient, and can actually be done while building the hierarchy.

5. Implementation

The input of our algorithm is a scalar field f given on any discretization that can be represented using a cell complex, e.g., a tetrahedral mesh or a regular 3D lattice. The latter allows for a very memory efficient implementation, since node/edge indices and neighborhood relations are implicitly given [GRP*12]. Let n denote the number of vertices of the cell complex, and let c denote the number of critical points of V_0. We follow a rather common pipeline (e.g. [GRP*12])

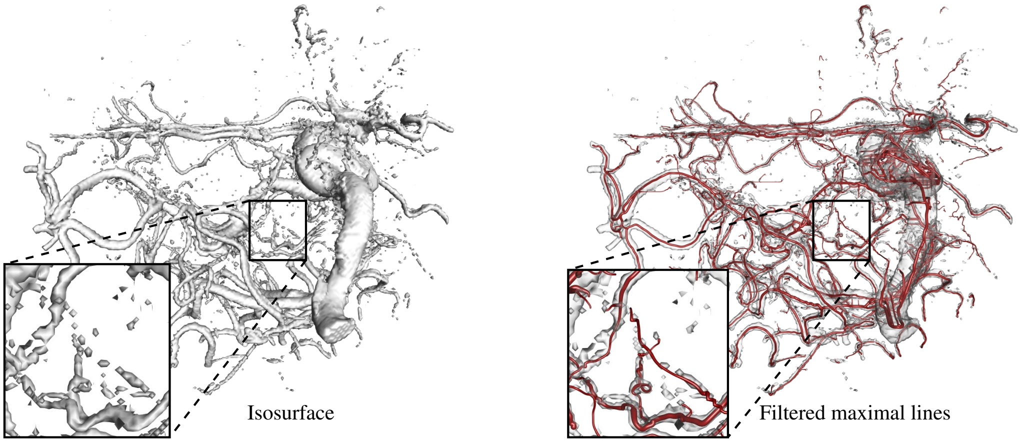

Figure 12: Extraction of extremal lines in a CT-scan of an aneurism using separatrix persistence.

to extract the extremal lines and surfaces of f. The computation of their separatrix persistence is woven into this:

1. **Initial MS complex:** We use the algorithm *ProcessLowerStar* by Robins et al. [RWS11] to compute the initial combinatorial gradient field V_0. The computational effort is $O(n)$ and it allows also for a parallel computation.
2. **Persistence:** Since the persistence homology of the cell complex and the MS complex of V_0 coincide, we can compute the persistence of the critical points directly on the MS complex itself [RWS11] with a complexity of $O(cn+c^3)$ [GRWH11].
3. **Hierarchy:** The hierarchy (V_i) is constructed as discussed in Section 3.4. The computational effort depends on the topological complexity, i.e., the number of critical points and their connectivity, with a worst-case complexity of $O(n^3)$. However, in practical cases the behavior is almost linear [GRP*12].

   During hierarchization, we compute separatrix persistence as discussed in Section 4.3.
4. **Geometric embedding:** Finally, the extremal lines and surfaces are written out by traversing (V_i) in reverse order. The computational effort depends on the size of the structure, but is at most $O(n)$.

For the final step, we found it beneficial to consider only the topological structures above an ε-persistence threshold to disregard small-scale structures. In our experiments, we set ε to 10 percent of the data range. This worked out for all of our experiments. However, this parameter depends on the application and needs to be adapted to the purpose of investigation. Since this parameter affects only the output and not the computation itself, this adaption can be easily done.

Note that different types of separation lines/surfaces share cells of the same dimension in the cell complex. This is by definition, see Section 3.2. Since these features are independent from each other, we use four sparse containers to store separatrix persistence individually for minimal/maximal lines and repelling/attracting surfaces together with a reference to the corresponding cell.

Given the extraction result, the user chooses an appropriate threshold for separatrix persistence to filter noise-induced and less important (parts of) extremal lines and surfaces. After filtering by separatrix persistence, we remove small isolated lines and surfaces.

Due to the combinatorial nature of our algorithm, the extracted lines and surfaces reflect the discrete nature of Ω, see the line wiggling in the close-up of Figure 15b or the discrete surface in Figure 16. To obtain visually pleasing results, we apply simple heat diffusion smoothing for surfaces and Bézier curve-based smoothing for lines. Note that a strong heat diffusion smoothing yields a shrinking of the surface, and Bézier curves are not able to capture kinks. We manually adjusted the smoothing strength such that these deviations can be neglected in our investigations.

6. Results

All results have been computed on a machine with an Intel Xeon E31225 (3.1GHz) CPU and 16 GB RAM. The timings given in Table 1 show the computation times needed to compute the initial MS complex, persistence of critical points, and the *complete* hierarchy (V_i) including separatrix persistence. Note that the computation time depends strongly on the topological complexity of the data set, i.e., the number of critical points and their connectivity (see also Section 5).

Aneurism Computer tomography (CT) scans usually suffer from a large amount of noise as it can be seen in the isosurface visualization of an aneurism in Figure 12 (left): filigree structures such as blood vessels are interrupted and represented by scattered surfaces. We applied our method with

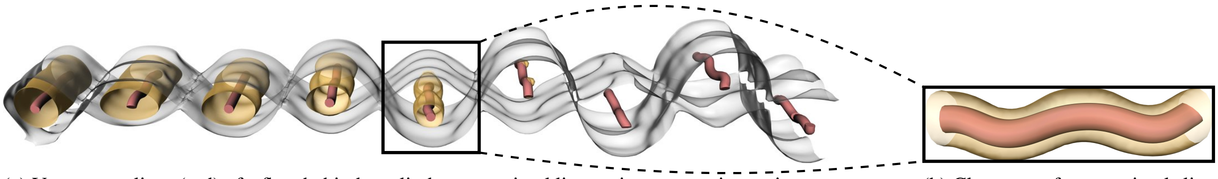

(a) Vortex core lines (red) of a flow behind a cylinder as maximal lines using separatrix persistence.

(b) Close-up of a maximal line (red) extracted using our method.

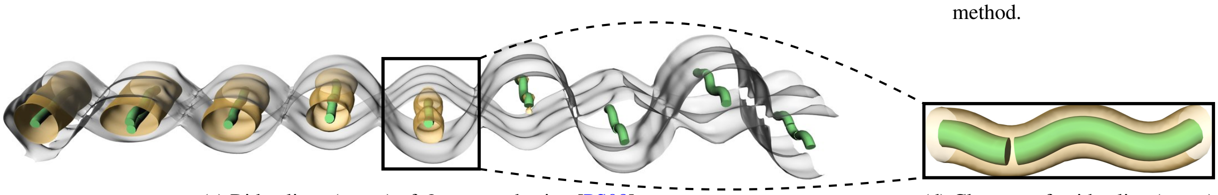

(c) Ridge lines (green) of Q extracted using [PS08].

(d) Close-up of a ridge line (green) extracted using [PS08].

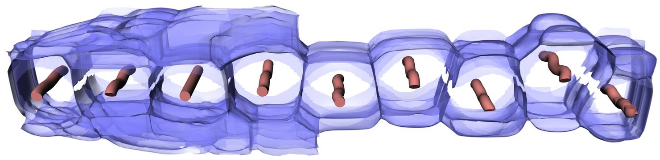

(e) The attracting surfaces (blue) of Q are a part of the *strain skeleton* for $Q < 0$ [SWTH07]. They partition the domain into vortex regions. Inside these regions, maximal lines (red) of Q are shown, i.e., lines of maximal vortical behavior. Lines/surfaces extracted using our method.

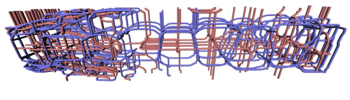

(f) All extremal lines of V_0.

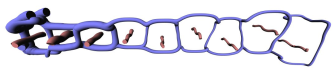

(g) Most dominant extremal lines filtered and scaled by separatrix persistence.

Figure 13: 3D unsteady flow behind a cylinder. Shown are extremal features of the Q-criterion for $t = \pi$. The gray isosurface depicts the zero-level of Q while the level $Q = 2.7$ is illustrated as yellow isosurface.

the goal to extract blood vessels as maximal lines. Figure 12 (right) shows the smoothed result filtered and scaled by separatrix persistence. Even in the presence of noise, connected blood vessels are robustly extracted.

Cylinder Flow Figure 13 demonstrates the results of our method applied to a scalar quantity derived from a flow behind a cylinder. The data set was provided by Bernd R. Noack (TU Berlin) from a direct numerical Navier Stokes simulation by Gerd Mutschke (FZ Rossendorf). It resolves the so called “mode B” of the 3D cylinder wake at a Reynolds number of 300 and a spanwise wavelength of 1 diameter. The data is provided on a $265 \times 337 \times 65$ curvilinear grid as a low-dimensional Galerkin model. The examined time range is $[0, 2\pi]$. The flow exhibits periodic vortex shedding leading to the well known von Kármán vortex street [ZFN*95]. This phenomenon plays an important role in many industrial applications, like mixing in heat exchangers or mass flow measurements with vortex counters. However, this vortex shedding can lead to undesirable periodic forces on obstacles, like chimneys, buildings, bridges and submarine towers.

We analyze the Q-criterion [Hun87] of this flow, which is a derived scalar field that allows to distinguish between vortex ($Q > 0$) and strain ($Q < 0$) behavior. The latter measures the amount of stretching and folding which drives mixing to occur. As pointed out by Sahner et al. [SWTH07], the minimal points/lines/surfaces of Q represent the *strain skeleton*, while the maximal features of Q denote the *vortex skeleton*.

Figures 13f-g provide a comparison between the unfiltered extremal lines and the lines filtered and scaled by separatrix persistence. Minimal lines are shown in blue, maximal lines in red. This exemplifies that separatrix persistence is able to reveal the most dominant features. We additionally applied a derived filter criterion here: the variance of separatrix persistence along a line. The idea is to favor lines that stay in the center of a vortex, i.e., that have a rather constant Q-value and therefore a rather constant separation strength.

The most dominant maximal lines and ridges of Q are shown in Figures 13a and 13c, respectively. The ridge lines are filtered by the F_{45} filter [PS08]. We additionally removed small isolated lines. Both extraction methods yield qualitatively very similar results. However, the close-ups in Figures 13b and 13d reveal an important difference of the two approaches: The topological approach gives long, fully connected lines (Figure 13b). In contrast, ridge lines are often split into several smaller parts in this data set (Figure 13d).

(a) All ridges.

(b) Filtered by F_{45}.

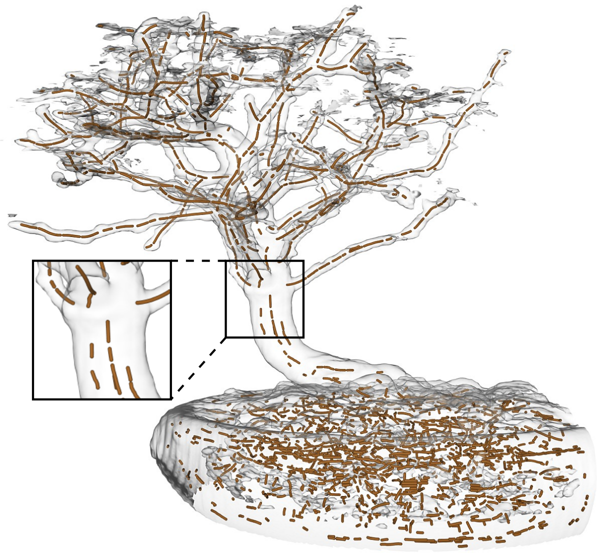

(c) Ridges restricted to the volume with $f > 55$.

Figure 14: Height ridges of the Bonsai data set.

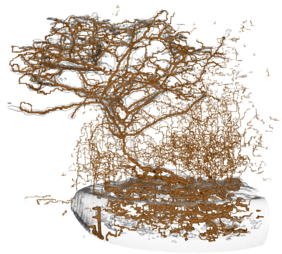

(a) All maximal lines scaled by separatrix persistence.

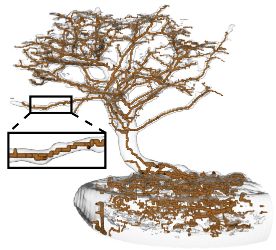

(b) Filtered by separtrix persistence.

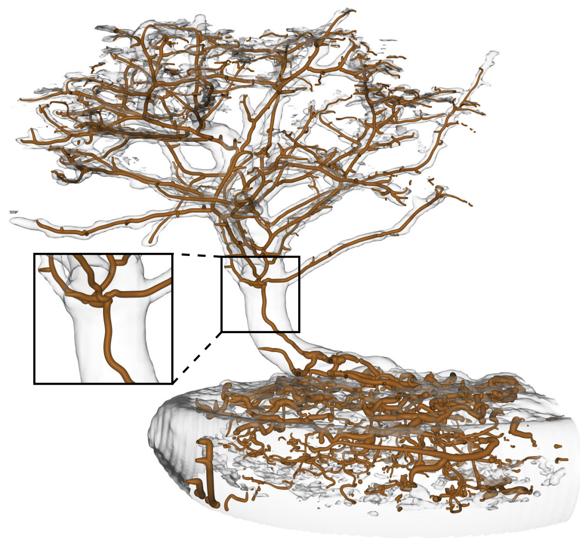

(c) Most dominant smoothed maximal lines.

Figure 15: Maximal lines of the Bonsai data set.

This is due to the fact that ridge lines are local features, i.e., it is locally decided whether or not a point is on a ridge or not. Due to numerical instabilities or noise, some of the local decisions along a ridge line may produce a “miss”, which then leads to disconnected results. This cannot happen for the topological approach, since separatrices are global features. On the other hand, ridge lines do not suffer from deviations due to smoothing.

Figure 13e shows the attracting surfaces of Q restricted to $Q < 0$. Following Sahner et al. [SWTH07], this provides a partition of the domain into vortex regions, which is nicely confirmed by the shown vortex core lines in the center of each of these regions.

Bonsai Figures 14 and 15 show the results of [PS08] and our method, respectively, applied to a CT-scan of a Bonsai tree. The objective in this data set is the extraction of the tree-skeleton – the trunk with all its branches. It appears as lines of maximal intensity in the CT-scan.

To extract the ridge lines, we first had to smooth this data set using a Gaussian filter. This reduced the noise level such that we were able to extract a meaningful result. The ridge definition alone yields a wealth of scattered lines, where the trunk and the tree are not identifiable, see Figure 14a. Therefore, we applied the filter criterion F_{45} [PS08]. While this reduced the complexity of the extraction result, the trunk and its branches are still not detectable, see Figure 14b. We restricted the ridge computation to regions with $f > 55$. Using this restriction, the overall structure of the tree becomes visible. However, the branches and the trunk are still represented by a scattered set of lines, see Figure 14c.

We applied all topological computations to the original data set (no smoothing). The result is shown in Figure 15a, where we show *all* maximal lines scaled by separatrix per-

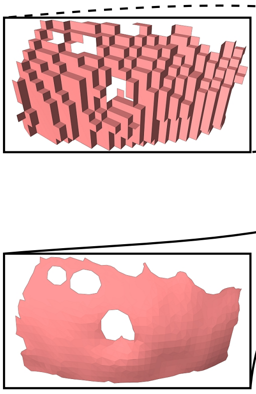

Figure 16: Discrete (top) and smooth (bottom) representation of a subregion of the cell membrane.

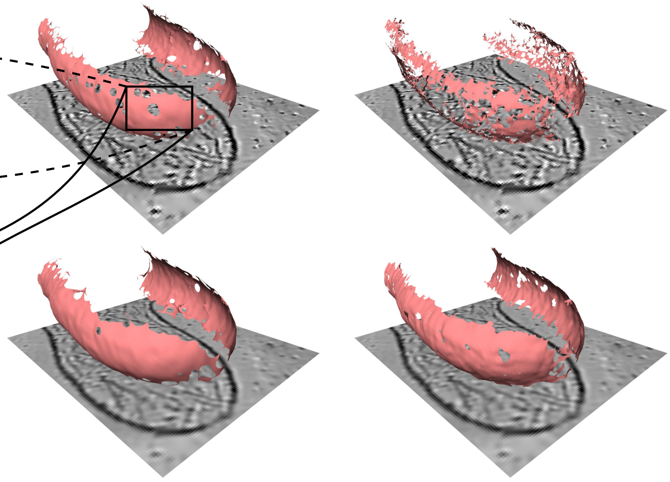

Figure 17: Extraction of a cell membrane in a cryo-electron tomogram using separatrix persistence (left column) and ridge/valley definition (right column). The top row shows the original data. The bottom row shows the results after Gaussian smoothing.

sistence. While the overall scenery is quite complex, the structure of the tree is already identifiable. Figure 15b shows the result after filtering by separatrix persistence. Due to the combinatorial nature of our method, the maximal lines follow the grid structure as it can be seen in the close-up of Figure 15b. We smoothed the maximal lines to obtain a visually pleasing result, see Figure 15c. The smoothing introduced only slight deviations in the geometric embedding. Note how the trunk and its branches are nicely represented as a connected network in contrast to the ridge extraction result.

Filopodium Cryo-electron tomography allows to visualize sub-cellular structures such as cell membranes. This imaging technique suffers from a very low signal-to-noise ratio and artifacts arising from incomplete information ("missing wedge"), which makes an automated extraction of these structures very challenging. We applied our method to a subtomogram of a *Dictyostelium discoideum* cell [RGH*12] with the goal to extract the cell membrane as the dominant parts of the attracting surfaces.

The sub-tomogram shows the so-called *Filopodium* – a finger-like extension of the cell. Figure 17 (left, upper row) shows the result after filtering using separatrix persistence and smoothing the surface using heat diffusion (see Figure 16 for the effect of the surface fairing). Although some holes within the membrane occur, its overall shape is well recovered. As described in [RGH*12], the tomogram was already filtered using non-local means. However, this filtering is not sufficient for the extraction of ridge surfaces as shown in Figure 17 (right, upper row): the membrane is only represented by a scattered set of small surface pieces. The remaining noise level challenges the ridge computation, in contrast to the topological approach. We applied Gaussian smoothing to lower the noise level further. The bottom row of Figure 17 shows the results for the smoothed version. Both extraction approaches benefit from this smoothing step. The cell membrane is almost closed, only few holes remain.

7. Conclusion and Future Work

We presented the – to the best of our knowledge – first topologically motivated measure of feature strength for separatrices of a 3D scalar field: *separatrix persistence*. It allows to filter noise-induced and less important extremal lines and surfaces. We compared our measure to the concept of *Height Ridges* on data sets from fluid dynamics, computer tomography and cell biology. The global nature of separatrix persistence, and the fact that it can be computed purely combinatorially without any need for derivatives, makes it very robust even in the presence of noise. The computation of separatrix persistence is woven into the common topological simplification process with only a small overhead, since existing information is reused. Furthermore, the computation of separatrix persistence is free of parameters, which allows for batch computations without any user interaction.

The topological simplification is currently the most time-consuming part of our extraction pipeline. We want to address this in future work by considering parallel computation approaches. This is a highly non-trivial issue, since topological simplification is an inherently global process. A first step in this direction has been presented in [GNPH07], but separation surfaces are not treated by that approach. Furthermore, we currently smooth the discrete extraction results using methods based on heat equation or Bézier curves. Although this smoothing is able to obliterate the discrete nature of the combinatorial separatrices, it introduces deviations in their geometric embedding, which could result in an intersection of them. It is therefore beneficial to investigate feature-based approaches in more detail that allow for error-controlled smoothing. Especially, constrained least-square approximations could be promising.

Acknowledgements The electron tomogram of a filopodium was generously provided by the Max Planck Institute of Biochemistry. The authors wish to thank the anonymous reviewers for their valuable comments and Jan Reininghaus for fruitful discussions.

References

[BLW11] BAUER U., LANGE C., WARDETZKY M.: Optimal topological simplification of discrete functions on surfaces. *Discrete & Computational Geometry* (2011), 1–31. 4, 7

[Cha00] CHARI M. K.: On discrete Morse functions and combinatorial decompositions. *Disc. Math. 217* (2000), 101–113. 3

[CSEH07] COHEN-STEINER D., EDELSBRUNNER H., HARER J.: Stability of persistence diagrams. *Discrete and Computational Geometry 37* (2007), 103–120. 4

[Dam99] DAMON J.: Properties of ridges and cores for two-dimensional images. *J. Math. Im. Vis. 10* (1999), 163–174. 2

[DLL*10] DEY T. K., LI K., LUO C., RANJAN P., SAFA I., WANG Y.: Persistent heat signature for pose-oblivious matching of incomplete models. *CGF 29*, 5 (2010), 1545–1554. 5

[dSV52] DE SAINT-VENANT B.: Surfaces à plus grande pente consituées sur les lignes courbes. *Bulletin de la soc. philomath. de Paris* (1852). 2

[Ebe96] EBERLY D.: *Ridges in Image and Data Analysis*. Kluwer Acadamic Publishers, Dordrecht, 1996. 2

[ELZ02] EDELSBRUNNER H., LETSCHER D., ZOMORODIAN A.: Topological persistence and simplification. *Discrete & Computational Geometry 28*, 4 (2002), 511 – 533. 1, 4

[For98] FORMAN R.: Morse theory for cell-complexes. *Advances in Mathematics 134*, 1 (1998), 90–145. 1, 3, 4

[For02] FORMAN R.: A user's guide to discrete Morse theory. Séminaire Lotharingien de Combinatoire, B48c, 2002. 3

[FP01] FURST J. D., PIZER S. M.: Marching ridges. In *Proc. IASTED International Conference* (2001), pp. 22–26. 2

[GNP*05] GYULASSY A., NATARAJAN V., PASCUCCI V., BREMER P.-T., HAMANN B.: Topology-based simplification for feature extraction from 3d scalar fields. In *Proc. IEEE Visualization* (2005), pp. 535–542. 3

[GNPH07] GYULASSY A., NATARAJAN V., PASCUCCI V., HAMANN B.: Efficient computation of Morse-Smale complexes for three-dimensional scalar functions. *TVCG 13*, 6 (2007). 11

[GRP*12] GÜNTHER D., REININGHAUS J., PROHASKA S., WEINKAUF T., HEGE H.-C.: Efficient computation of a hierarchy of discrete 3d gradient vector fields. In *Topo. Methods in Data Analysis and Vis. II*. Springer, 2012, pp. 15–30. 3, 5, 7, 8

[GRWH11] GÜNTHER D., REININGHAUS J., WAGNER H., HOTZ I.: Memory efficient computation of persistent homology for 3D image data using discrete Morse theory. In *Proc. SIBGRAPI* (2011), pp. 25–32. 3, 8

[Hat02] HATCHER A.: *Algebraic Topology*. Cambridge University Press, Cambridge, U.K., 2002. 3

[Hun87] HUNT J.: Vorticity and vortex dynamics in complex turbulent flows. *Proc CANCAM, Trans. Can. Soc. Mec. Engrs 11* (1987), 21. 9

[JP06] JOSWIG M., PFETSCH M. E.: Computing optimal Morse matchings. *SIAM J. Discret. Math. 20*, 1 (2006), 11–25. 5

[Kv93] KOENDERINK J., VAN DOORN A.: Local features of smooth shapes: ridges and courses. In *Proc. SPIE Geometric Methods in Computer Vision II* (1993), vol. 2031, pp. 2–13. 2

[Lew12] LEWINER T.: Critical sets in discrete morse theories: Relating forman and piecewise-linear approaches. *Computer Aided Geometric Design*, 0 (2012), –. 3

[LLSV99] LOPEZ A., LUMBRERAS F., SERRAT J., VILLANUEVA J.: Evaluation of methods for ridge and valley detection. *Pattern Analysis and Machine Intelligence, IEEE Transactions on 21*, 4 (apr 1999), 327 –335. 2

[LLT03] LEWINER T., LOPES H., TAVARES G.: Optimal discrete Morse functions for 2-manifolds. *Comput. Geom. Theory Appl. 26* (November 2003), 221–233. 3

[Max70] MAXWELL J. C.: On hills and dales. *The London, Edinburg and Dublin Philosophical Magazine and Journal of Science 40* (1870), 421–425. 2

[Mil63] MILNOR J.: *Morse Theory*. Princeton University Press, 1963. 1, 3

[Mil65] MILNOR J.: *Topology from the differentiable viewpoint*. Univ. Press Virginia, 1965. 3

[NS94] NAJMAN L., SCHMITT M.: Watershed of a continuous function. *Signal Processing 38*, 1 (1994), 99 – 112. 1

[POS*11] PAGOT C., OSMARI D., SADLO F., WEISKOPF D., ERTL T., COMBA J.: Efficient parallel vectors feature extraction from higher-order data. *CGF 30*, 3 (2011), 751–760. 2

[PR99] PEIKERT R., ROTH M.: The parallel vectors operator - a vector field visualization primitive. In *Proc. IEEE Visualization* (1999), pp. 263–270. 2

[PS08] PEIKERT R., SADLO F.: Height Ridge Computation and Filtering for Visualization. In *Proc. PacificVis* (2008), pp. 119 – 126. 2, 9, 10

[RGH*12] RIGORT A., GÜNTHER D., HEGERL R., BAUM D., WEBER B., PROHASKA S., MEDALIA O., BAUMEISTER W., HEGE H.-C.: Automated segmentation of electron tomograms for a quantitative description of actin filament networks. *Journal of Structural Biology 177*, 1 (2012), 135–144. 1, 11

[RWS11] ROBINS V., WOOD P., SHEPPARD A.: Theory and algorithms for constructing discrete Morse complexes from grayscale digital images. *IEEE Trans. on Pattern Analysis and Machine Intelligence 33*, 8 (2011), 1646–1658. 8

[Sma60] SMALE S.: On dynamical systems. *Boletín de la Sociedad Matemática Mexicana 5*, 2 (1960), 195–198. 2

[SPFT12] SCHINDLER B., PEIKERT R., FUCHS R., THEISEL H.: Ridge concepts for the visualization of Lagrangian coherent structures. In *Topological Methods in Data Analysis and Visualization II*. Springer, 2012, pp. 221–235. 2

[SWTH07] SAHNER J., WEINKAUF T., TEUBER N., HEGE H.-C.: Vortex and strain skeletons in eulerian and lagrangian frames. *IEEE TVCG 13*, 5 (2007), 980–990. 1, 2, 9, 10

[Wei08] WEINKAUF T.: *Extraction of Topological Structures in 2D and 3D Vector Fields*. PhD thesis, U. Magdeburg, 2008. 1, 3

[WG09] WEINKAUF T., GÜNTHER D.: Separatrix Persistence: Extraction of salient edges on surfaces using topological methods. *CGF 28*, 5 (2009), 1519–1528. 1, 2, 5

[ZFN*95] ZHANG H.-Q., FEY U., NOACK B., KÖNIG M., ECKELMANN H.: On the transition of the cylinder wake. *Phys. Fluids 7*, 4 (1995), 779–795. 9